Punching Capacity of UHPC Post Tensioned Flat Slabs with and Without Shear Reinforcement: An Experimental Study

Ahmed Afifi [1], Mohamed Ramadan [1, 2], Ahmed M. Farghal Maree [2],
Ahmed M. Ebid [3*], Amr H. Zaher [2], Dina M. Ors [3]

[1] *Faculty of Engineering, October 6 University, Giza Governorate, Egypt.*

[2] *Faculty of Engineering, Ain Shams University, Cairo, Egypt.*

[3] *Faculty of Engineering and Technology, Future University in Egypt, New Cairo 11865, Egypt.*

Abstract

Punching capacity is one of the main items in the design of both pre-stressed and non-pre-stressed flat slabs. All international design codes include provisions to prevent this type of failure. Unfortunately, there is no code provision for UHPC yet, and hence, the aim of this research is to experimentally investigate the impact of column dimensions and punching reinforcement on the punching capacity of post-tensioned slabs and compare the results with the international design codes' provisions to evaluate its validity. The test program included five slabs with a compressive strength of 120 MPa: one as a control sample, two to study the effect of column size, and the last two to study the effect of punching reinforcement. Comparing the results with the design codes showed that ACI-318 is more accurate with an average deviation of about 5%, while EC2 is more conservative with an average deviation of about 20%. Besides that, punching reinforcement reduces the size of the punching wedge by increasing the crack angle to 28° instead of 22° for slabs without punching reinforcement. Also, the results assure that both ductility and stiffness are enhanced with the increased column dimensions and punching reinforcement ratio.

Keywords: Ultra-High-Performance Concrete; Post-Tensioning; Flat Slabs; Punching Shear.

1. Introduction

Ultra-High-Performance Concrete (UHPC) is a new advanced concrete that has been transferred from laboratory research to practical applications. Based on the latest developments in concrete technology, UHPC is characterized by extraordinary mechanical properties in terms of high compressive and tensile strengths, high Young's modulus, and excellent durability and workability when compared with normal or high-strength concrete. Using steel fibers is recommended in the UHPC mix design to enhance ductility [1, 2].

UHPC with high compressive strength and improved workability and durability mark a quantum leap in concrete technology. This high-performance material offers a combination of exciting applications. It permits the construction of endurable and economical buildings with extraordinarily ultra-thin designs. Its high strength makes it a suitable building material for bridge decks, storage halls, thin-wall shell structures, and highly loaded structural elements.

Nowadays, reinforced concrete flat slabs have been widely used in residential and commercial buildings for their architectural advantages in terms of larger clear heights, faster construction with simplified formwork, and minimum

---

depth [3–5]. Also, flat slabs have proven their ability to upgrade or alter the existing structural system to increase the number of stories in a building. Even though flat slabs still have a concern regarding the high-stress centration at column-slab joints, which significantly affects the punching shear problem.

Over the past few decades, rapid development and huge-scale building construction have taken place in several countries, and due to their low cost and high durability requirements, post-tension flat slabs are broadly used in such countries as they meet most of what clients and engineers require. Additionally, the post-tensioned flat slabs offer more economical and flexible solutions than normal reinforced concrete. For the same span length, post-tensioned flat slabs are usually thinner than normal reinforced ones, and hence, the punching phenomenon becomes more serious. Post-tensioning allows for longer clear spans, thinner slabs, and fewer beams, which result in a smaller amount of concrete and a lower weight of the overall structure. However, small slab thickness and a smaller number of columns lead to higher column loads and a higher potential of punching failure in the slab [6, 7].

The problem of punching shear is a main item in designing flat slabs. The relatively abrupt nature of failure in shear, as compared to a ductile flexural failure, makes it desirable to design members so that strength in shear is relatively equal to or greater than strength in flexure, to ensure that a ductile flexural failure precedes shear failure [8]. Thus, so much research work has been developed to investigate the various techniques that can be applied to enhance the punching shear of the reinforced concrete flat slabs.

Azmee & Shafiq (2018) [9] summarized the advantages of the applications of ultra-high-performance concrete as a basic future building material. The authors found that this innovative material's use is still limited for so many reasons, including and not limited to the high initial cost, limited available design codes, complex fabrication, and limited available resources. Wu et al. 2019, [10] conducted a parametric study using a validated finite element model to investigate the effect of using an overlay layer of UHPC on the punching shear behavior. This analytical investigation revealed that the effects of the reinforcement ratio and the steel yield strength have little effect on the punching ultimate load and the corresponding deflection as well. Furthermore, the thickness and strength of the UHPC layer are the key parameters that control the punching shear behavior of the flat overlayed plates. The authors considered that these parameters effects could be linearly influenced by the punching shear capacity of the composite overlayed flat plates.

Inácio et al. (2020) [11] experimentally tested a series of composite flat slabs consisting of a normal-strength concrete layer at the compression zone and topped with high-strength concrete that reached 120 MPa and extended to 1.50, or 3 times the flat slab thickness. The authors found that for rational use of high-strength concrete, a minimum thickness of normal-strength concrete is 50 mm for constructive reasons and can be increased according to the depth of the compression zone. Also, the layer of high-strength concrete extending a distance equal to two times the slab thickness from the column edge is effective enough to enhance the punching shear ultimate load and the corresponding delayed deflection.

Menna & Genikomsou (2020) [12] developed a 3D finite element model to investigate the influence of retrofitting the column-slab joint with ultra-high performance fiber reinforced concrete (UHPFRC) on the punching shear behavior. Researchers found that placing a thin layer of the UHPFRC on the tension side of the slab-column connection increased the punching shear strength, which is proportional to the layer thickness. Also, installation of the retrofitting layer at the critical punching area only achieves a more ductile, effective, and sustainable solution.

Dogu & Menkulasi (2020) [13] experimentally tested a series of unbonded posttensioned flexural members under the effect of three loading points. Authors also developed a prediction finite element model for the ultimate failure load of the members made of ultra-high-performance concrete with various statical systems and shear span-to-depth ratio.

Isufi & Ramos (2021) [14] highlighted the gaps between the previous research work to determine the required future studies that would lead to improving the knowledge of ultra-high-performance concrete (UHPC) in flat slabs. Authors found that several other fiber materials exist, but their applicability on real-scale members susceptible to punching shear failure has not been sufficiently explored. A current research paper is part of this recommended research work.

Sharma et al. (2022) [15] investigated the influence of the chloride and acid attack on the behavior of concrete with high compressive strength. The authors found that loss of compressive strength is decreased with the increase in the concrete grade when exposed to severe environmental conditions as the exposure of chloride or acidic attack.

Muhammed & Karim (2022) [16] experimentally studied the behavior of internally supported UHPC flat slabs with drop panels. Specimens varied in the area covered by the drop panel around the column, which ranged between 10.5% to 19% of the total flat slab area. The authors found that the zone of 10.5% achieved improved punching shear behavior in terms of delayed deflection values and limited strain in the steel reinforcement and concrete.

Elsayed et al. (2022) [17] installed a layer of UHPC on flat slab sides. Slabs strengthened with a UHPC layer in the compression side extending to half the slab depth away from the adjacent column exhibited more punching shear strength when compared with flat slabs without retrofitting and slabs with a layer in the tension side. Also, the authors developed a theoretical approach that agreed very well with the experimental test results.

Gołdyn & Urban (2022) [18] applied hidden column capitals made of UHPC to LWRC flat slabs to enhance the punching shear ultimate load. Slabs with column heads increased the ultimate load by 82% when compared to slabs without UHPC column heads. The researchers developed a theoretical approach to simulate punching behavior with ratios of theoretical to experimental load equal to 0.87 and 1.16.

Ebid & Deifalla (2022) [19] developed three models using different artificial intelligence techniques to predict the punching shear strength of the lightweight concrete flat slabs. The developed models included the effects of various parameters, including concrete density, column dimensions, slab depth, concrete strength, and reinforcement ratio by steel yield stress. The artificial intelligence models captured the true behavior and overcame the variability of the traditional design codes concerning the effective parameters.

Elsheshtawy et al. (2022) [20] investigated the effect of both layout and level of posttensioning on the punching shear behavior of normal reinforced concrete posttensioned flat slabs. The authors concluded that increasing the level of posttensioning significantly increased the punching capacity in both cases of distributed and bundled strand layout. Bundled strands significantly increased the flat slabs stiffness at all levels of prestressing.

Ramadan et al. (2023) [21] conducted an experimental study to investigate the effect of concrete compressive strength and the prestressing strands on the punching shear behavior of the ultra-high-performance concrete posttensioned flat slabs. The authors found that the increase of the concrete compressive strength delayed flat slab cracking before the brittle punching shear failure and significantly increased the punching shear strength with more ductile behavior. While the strands lay out highly influenced the flat slabs deformed shape in terms of flatter failure angle in case of bundled strands with less deflection values.

The previous literature review illustrates an investigation gap regarding the impact of both punching reinforcement and load aspect ratio on the punching capacity of a posttensioned (UHPC) flat slab. Hence, the main objective of this study is to fill this gap. The study is organized into six sections: the considered methodology is described in Section 2, while Section 3 explains the details of the experimental program, and test results are summarized in Section 4. The recorded results are analyzed, discussed, and compared with design codes in Section 5. Finally, Section 6 contains conclusions, limitations, and recommendations.

2. Research Methodology

The methodology considered in this research begins with collecting, sorting, and analyzing the previous work regarding UHPC, posttensioned flat slabs, and punching in flat slabs. The output of this stage indicated a gap study regarding the impact of punching reinforcement and aspect ratio of loaded area on the punching capacity of posttensioned UHPC flat slabs. Accordingly, the next stage is to design an experimental test program to investigate this gap. The developed test program contains five slabs: a control slab (S1), two slabs with different aspect ratios for loading area (S2, S3), and two slabs with different punching reinforcement percentages (S4, S5). The impact of the aspect ratio of the loading area is investigated by comparing the testing results of (S1, S2, and S3), while the effect of punching reinforcement is investigated using the results of (S1, S4, and S5). Finally, the recorded results are compared with the provisions of two international design codes (ACI-318 and EC2), and the research conclusions are summarized, including the study limitations and further research recommendations. Figure 1 shows the considered methodology.

3. Experimental Program

3.1. Specimens

Five bonded posttensioned concrete slabs were designed and fabricated to investigate the punching shear behavior under incremental vertical loading. All slabs had the same geometry (1000×1000×120 mm). The same posttensioning stress was applied to all slabs using four 0.50" strands in each direction. All the strands had an eccentricity of 25mm at midspan. Mild reinforcement bars were used behind the anchors to resist the tensile-splitting forces. The grade of the used strands was 270, with an ultimate strength (f_{pu}) of 1860 MPa, and the strands were tensioned to 0.75 of their ultimate strength. The anchorage slippage losses in pre-stressing force are significant due to short strands, as in this research. Thus, the specimens were designed with an excess length of 500 mm on each of the four sides to double the length of strands and keep the anchorage zone away from the punching zone. Figure 2 shows the concrete dimensions and strand profiles for all the tested slabs.
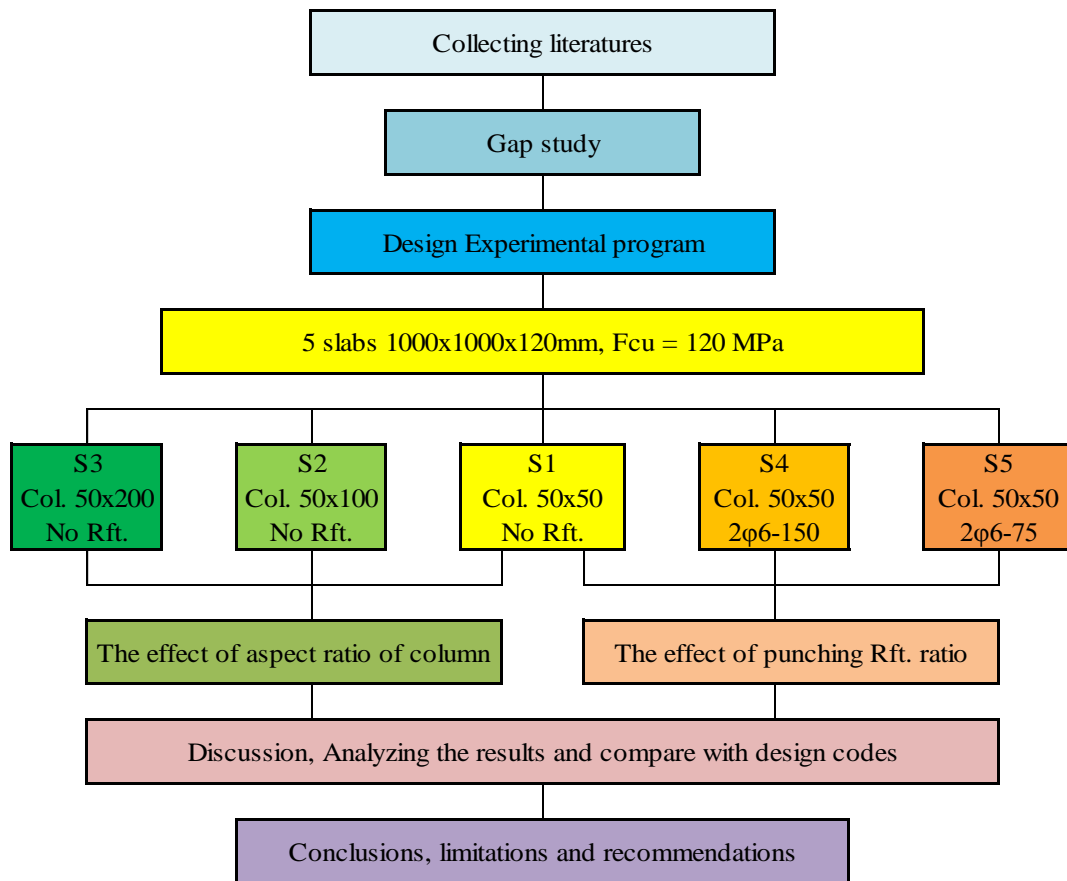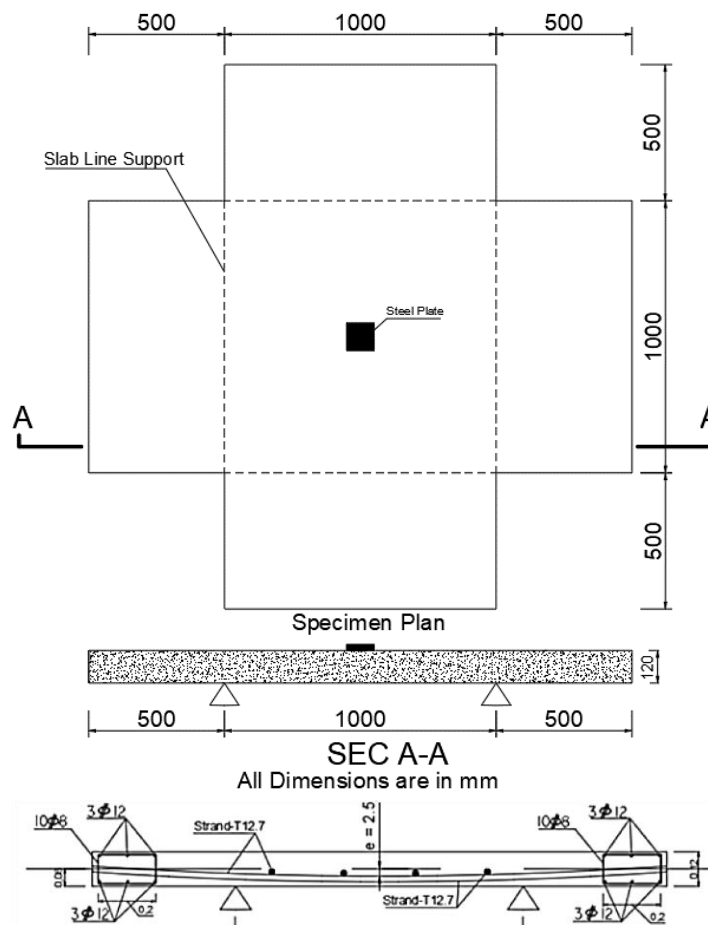
Figure 1. The considered methodology

Figure 2. Concrete dimensions for all slabs

Two parameters were studied in this research: column dimension and punching shear reinforcement ratio. Three different column dimensions were considered: (50×50 mm), (50×100 mm) and (50×200 mm) for specimens S1, S2, and S3 in order. The influence of punching shear reinforcement ratio on the shear strength was studied using three specimens (S1, S4, and S5) for unreinforced, reinforced with stirrups T6mm @ 150mm and T6mm @ 75mm, respectively, as shown in Figure 3. All slabs were gradually loaded with a vertical hydraulic jack onto a steel plate placed at the center of the slab. The characteristics of each slab regarding dimensions of the loading area and punching reinforcement are summarized in Table 1.
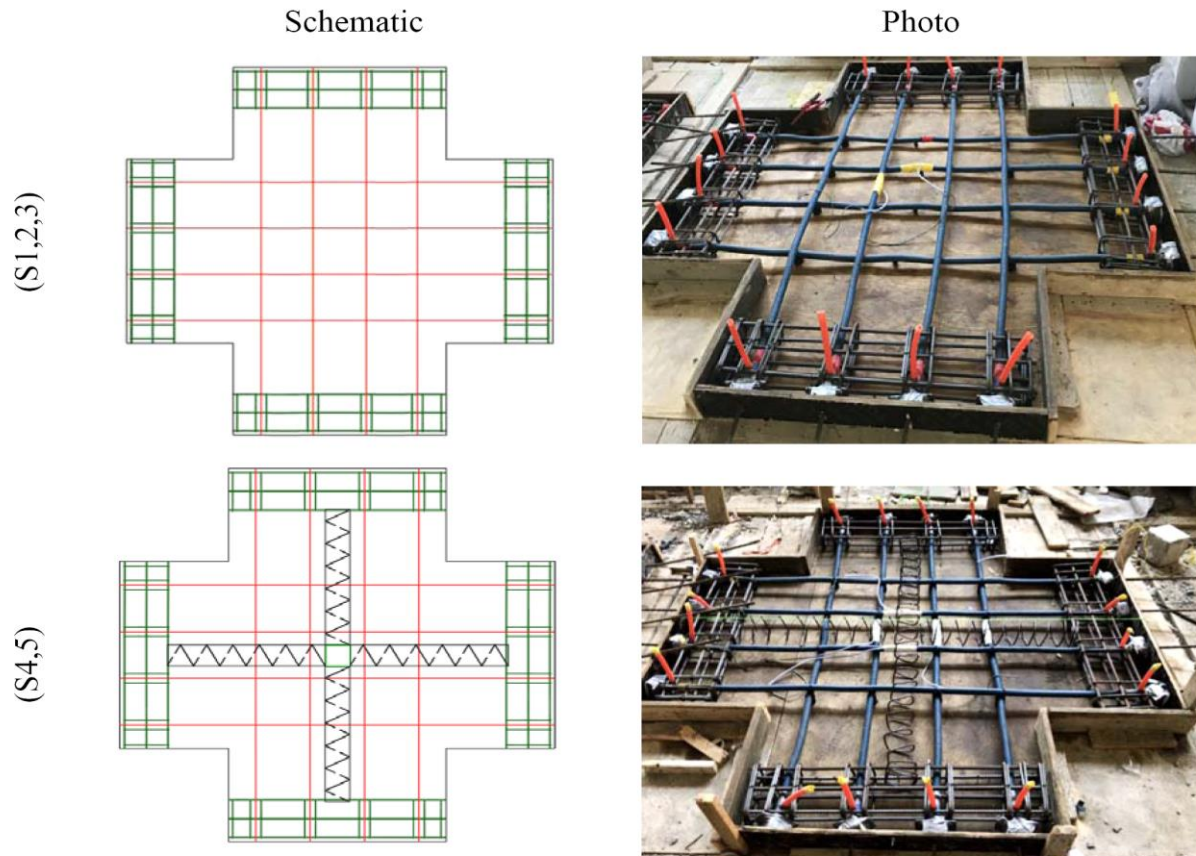

Figure 3. Strands and punching reinforcement layout

Table 1. Characteristics of tested slabs regarding dimensions of loading area and punching reinforcement

Slab ID	Dimensions (mm)	f_{cu} (MPa)	Dim. of Loading area (mm)	Shear Reinforcement per direction
S1			50 × 50	---
S2			50 × 100	---
S3	1000 × 1000 × 120	120	50 × 200	---
S4			50 × 50	2ɸ6@150 mm
S5			50 × 50	2ɸ6@75 mm

3.2. Materials

All slabs were casted using the same UHPC. The details of the mix are summarized in Table 2. Finely crushed dolomite stone (size between 2 to 6 mm) was used as coarse aggregate, and medium sand (size between 0.2 and 0.6 mm) was used as fine aggregate. In addition, the used Ordinary Portland Cement (OPC), silica fume, quartz powder, superplasticizer (*ViscoCrete*), and steel fibers were supplied [22–26]. Due to the low water cement ratio (W/C) used in this mix and to ensure homogeneity, a pan mixer was used as follows: fine materials (cement, silica fume, and quartz powder) were added and dry mixed together, then half the amount of mixing water was added gradually to the fines and mixing continued for two minutes. The superplasticizer is added to the remaining water and then added to the mix, and the mixing continues for three to four minutes till a homogenous paste is achieved. Finally, fine aggregate is

added gradually to the mix, followed by the coarse aggregate, and mixing continues for 5 to 6 minutes. After casting the specimens, they were left to harden for 24 hours in the formwork, then the slabs were cured with steam in a chamber with an average temperature 70° for a continuous seven days. Six concrete cubes 150×150×150 mm and three standard cylinders, 150 mm in diameter and 300 mm in height were cast alongside the slabs and cured with the same method. The average compressive strength (f_{cu}) of the six cubes and the average tensile strength (f_{ct}) of the three cylinders at testing time were 119 MPa and 10.5 MPa, respectively.

Table 2. Mix proportion of the used UHPC

CEM I 52.5N (kg/m³)	Silica fume (kg/m³)	Medium Sand (kg/m³)	Quartz Powder (kg/m³)	Fine Dolomite (kg/m³)	Water (kg/m³)	ViscoCrete (kg/m³)	Steel Fiber (kg/m³)
800	160	333	333	666	154	38.5	78.5

Low-relaxation, 7-wire strands, 0.5" diameter, and their corresponding accessories (mono-strand anchors, wedges, bearing plates, and corrugated plastic ducts) were used in all slabs. The used strands were compliant with ASTM A416 "Standard Specification for Steel Strand, Uncoated Seven Wire Strand for Prestressed Concrete" [27]. Four mild steel cages were installed at the anchorage zones to resist the splitting forces. Each cage consists of 3 top and 3 bottom longitudinal bars, 12 mm in diameter, and 10 stirrups, 8 mm in diameter, as shown in Figure 3. All strands were jacked to 75% of the ultimate capacity and grouted as soon as the concrete gained 75% of its characteristic strength. The losses due to 6 mm anchor slippage are about 600 MPa; hence, the actual stresses in the strands are about 0.75 × 1860-600 ≈ 800 MPa.

Slabs (S4, 5) were supplied with punching reinforcement as shown in Figure 3. The used reinforcement consists of four spiral square ties (60×60 mm), one in each direction. The pitches of the spiral ties were 150 and 75 mm for S4 and S5, respectively. The spiral ties were also mild steel ST (24/37), with a yield stress of 240 MPa and an ultimate strength of 370 MPa.

3.3. Test Setup and Instrumentation

The utilized testing setup shown in Figure 4 is located in the Reinforced Concrete Research Center at Ain Shams University, Cairo. All slabs were loaded at the center by a 1000 kN capacity hydraulic jack on the top surface through a steel loading block to simulate the column size. The slabs were resting on four steel I-beams at support lines (the dashed lines in Figure 2). The inner strands of each slab were provided by strain gauges in the middle to measure the forces in the strands. In addition, six LVDTs were fixed below the slab to measure the deflections: two below the loading block and four in the ¼ and ¾ of the span in both directions, as shown in Figure 5.
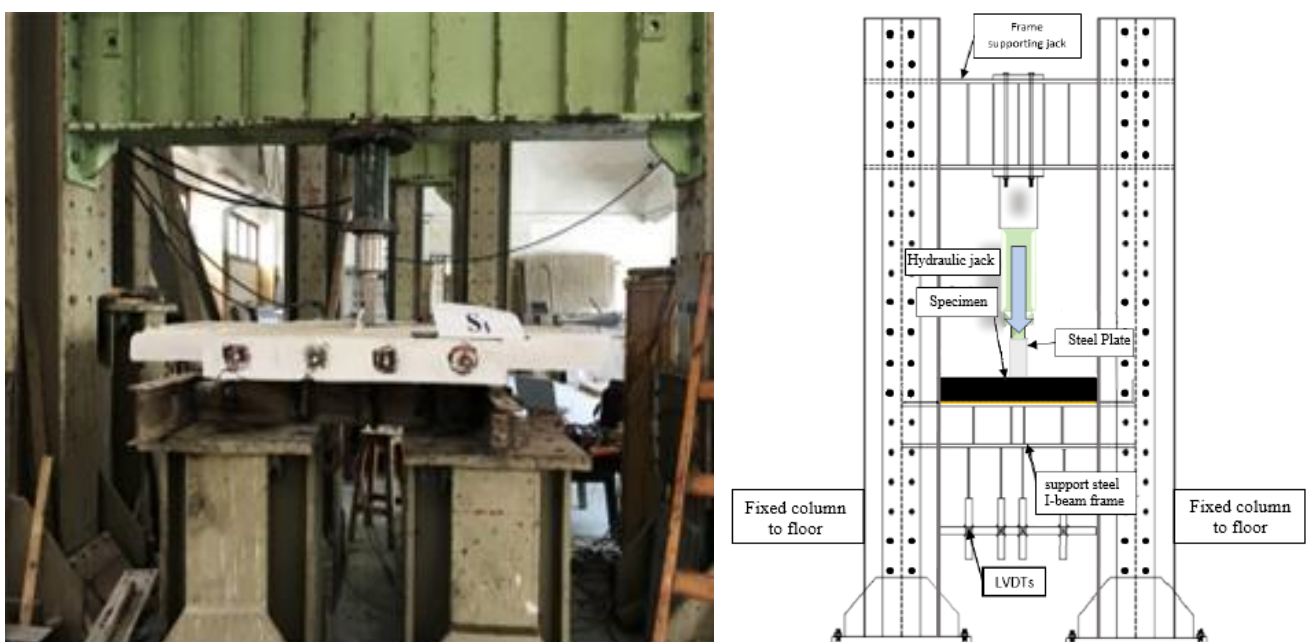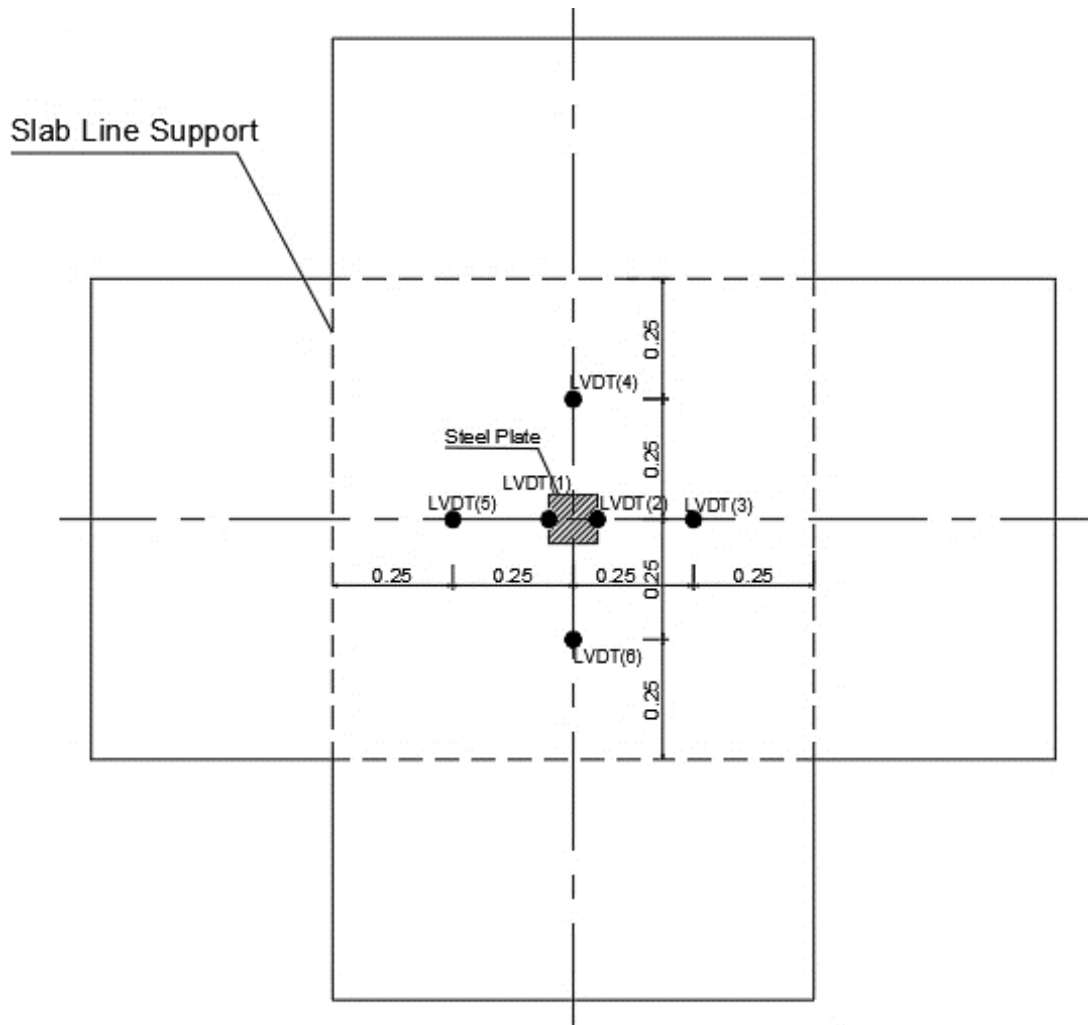

Figure 4. Test setup and loading system

Figure 5. LVTD's locations below the slab

4. Results

Each tested slab was gradually loaded, after each load step, the cracks on the lower surface were plotted and photographed, readings from both strain gages and LVTD's were automatically and continuously recorded using data acquisition system. All results are summarized in Table 3.

Table 3. Experimental results

Slab	Pcr kN	Pu kN	Δcr mm	Δu mm	ε_{cr} μ-strain	ε_{u} μ-strain
S1	100	245.0	2.7	12.7	18	869
S2	60	274.7	1.3	11.2	Damaged	
S3	90	327.4	1.4	10.2	90	2014
S4	70	271.4	2.1	11.2	96	1640
S5	95	341.5	1.6	11.9	Damaged	

Pcr: Load at 1st flexural crack; Pu: Load at ultimate stage; Δcr: The average mid span deflection at 1st flexural crack; Δu: The average mid span deflection at ultimate stage; ε_{cr}: The average strain in strands at mid span at 1st flexural crack; ε_{u}: The average strain in strands at mid span at the ultimate stage during testing excluding the initial prestressing strains.

For all tested slabs, the failure started with flexural hair cracks below the loading block and with increasing the load, the cracks' widths increased, and number of radial cracks increased until the punching shear failure suddenly happened with very loud noise and the hydraulic jack load decreased. Load-deflection curves for tested slabs are presented in Figure 6, while failed slabs photos and their crack pattern at 50%, 75% & 100% of the ultimate loads are showed in Figure 7.
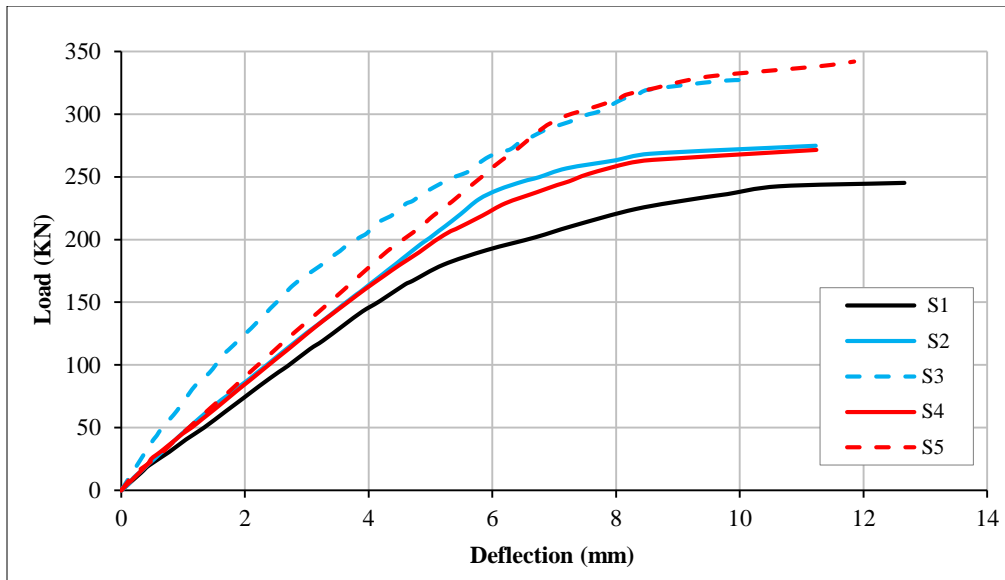
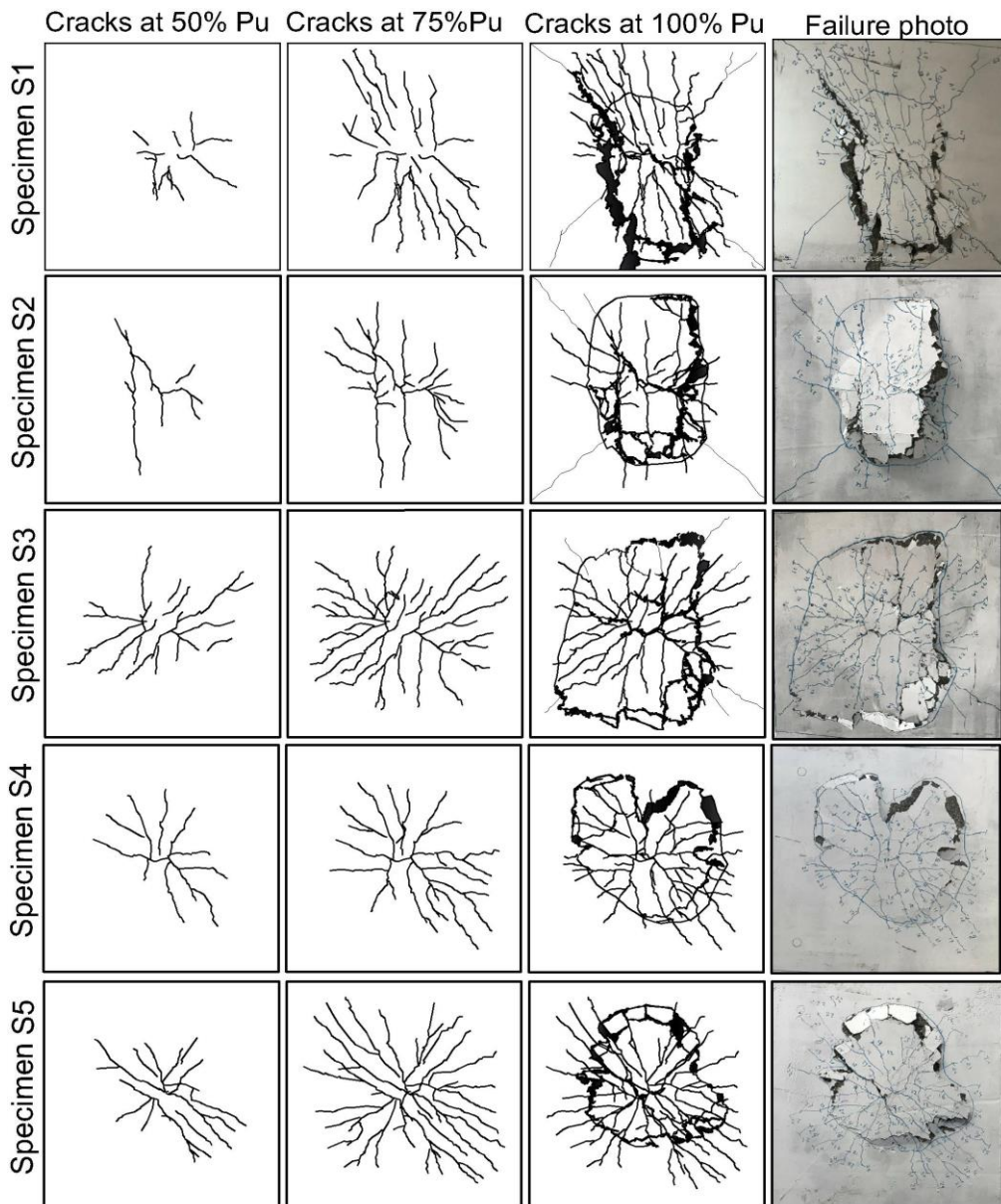**Figure 6. Load-deflection curves for tested slabs**

Figure 7. Crack pattern and failure photo for tested slabs

5. Discussions

5.1. Failure Pattern

Revising the experimental observations and measured strains indicated that all slabs failed in punching. As shown in Figure 7, the failure begins with limited flexural crakes below the loading block; then the diagonal cracks increased with increasing the load till the punching wedge formed and suddenly separated from the slab with a loud noise, and no cracks were observed on the top surface of the slabs. The measured strains in the strands at the ultimate stages, excluding the initial prestressing strains (4000 μ-strain), were 869, 1640, and 2014 μ-strain for slabs S1, 4, and 3, respectively, while strain gauges of specimens S2 and S5 were damaged during casting and/or grouting. These strains correspond to stresses in the stands of 974, 1128, and 1202 MPa, which are much less than the yield stress of the strands (1586 MPa), which assured that all slabs failed in pure punching.

The photos in Figure 7 indicated that the size and aspect ratio of the punching wedge depend on the column dimension and shear reinforcement ratio. The bottom surface area of the punching wedge of S3 (column dimensions 50×200 mm) is quite large (about 800×600 mm) compared with the areas of S1 and S2 (column dimensions 50×50 mm and 50×100 mm), which are almost similar (about 700×500 mm). On the other hand, shear reinforcement reduced the punching wedge to about (500×500 mm) and is almost circular. The plain concrete zones between strands in specimens (S1, S2, and S3) without shear reinforcement allow the punching cracks to propagate freely from the mid-height of the slab toward the upper and lower surfaces. Accordingly, the angle between the punching crack and the horizontal was about 22° for slabs without shear reinforcement and 28° for slabs with shear reinforcement.

5.2. First-Crack Load

Table 3 lists the recorded load at the first flexural crack for each tested slab. These loads represent the flexural capacity of the uncracked section of the slabs, which is a function of the tensile strength of concrete. Neglecting the contribution of stands, the modulus section of the slab is 0.0024 m^3, and considering the measured concrete tensile strengths (10.5 MPa), the expected first-crack load for all slabs is 100 KN. The measured values ranged between 60% and 100% of the calculated ones, with an average deviation of 17%. Figure 8 graphically presents these results.
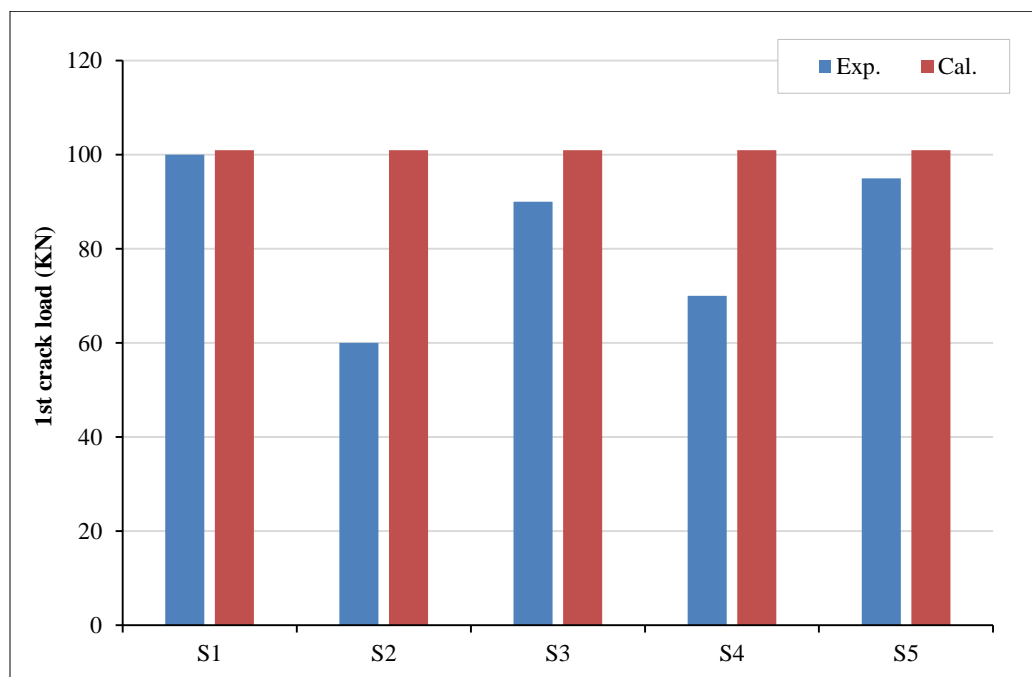

Figure 8. Experimental 1st cracks load vs. calculated ones

5.3. Punching Capacity

The theoretical punching capacities were calculated as per ACI-318-14 & EC2-04. Figure 9 illustrates both codes' critical punching section. The punching capacity formulas in ACI-318-14 [28] and EN 1992-1-1 [29] are presented in Equations 1 and 2 respectively.
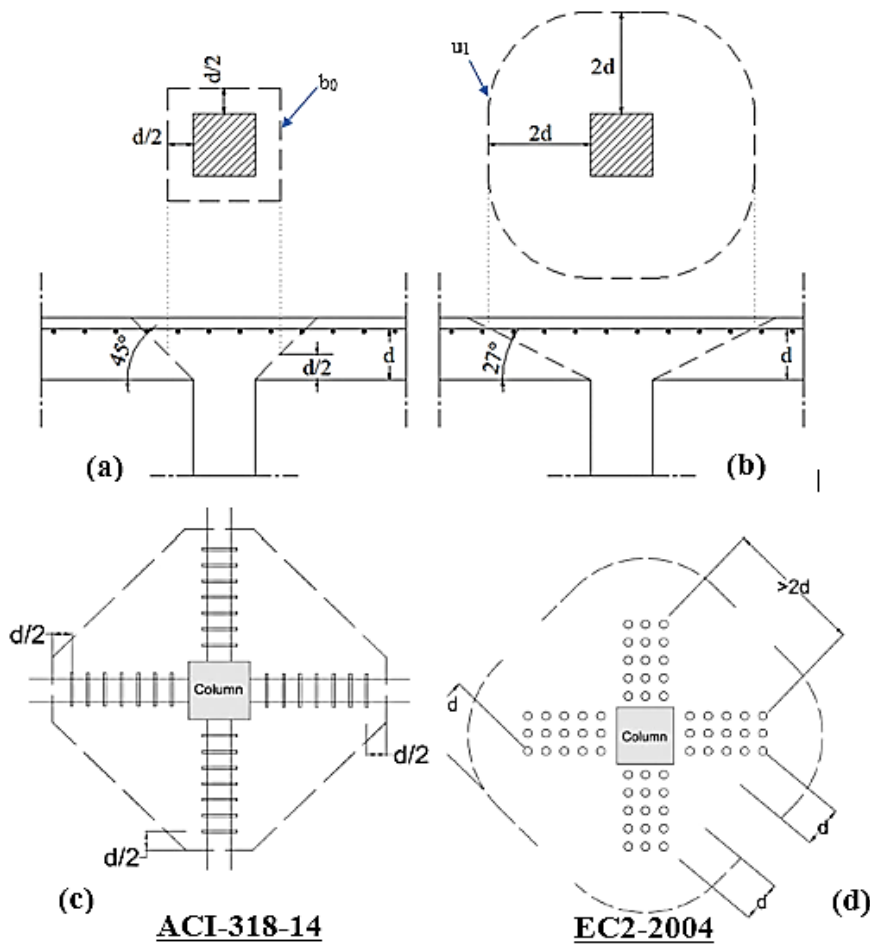
Figure 9. Critical punching section & the punching capacity formula (a and c) using ACI-318-14, (b and d) using EC2-2004

$$V_{ACI} = \beta_P \sqrt{f_c`}\, b_0 d + 0.3 f_{pc} b_0 d + V_p + \frac{A_v f_{yt}\, d}{s} \tag{1}$$

where V_{ACI} is Ult. Punching shear capacity (N), β_p is smaller of 0.29 and $0.083(\alpha s.d/bo+1.5)$, αs is 20, 30, and 40 for corner, edge, and internal columns, respectively; d is slab depth measured from extreme compression fiber to tension reinforcement centroid but not less than 80% of slab thickness; b_o is critical perimeter length at d/2 from column face; f_{pc} is mean prestress compressive stresses along the critical perimeter after all losses ≤ 3.5 MPa; V_p is the downward component of the prestressing tendons' force that are crossing the critical perimeter after all losses; $f_c`$ is cylinder compressive strength of concrete; S is the spacing of the shear reinforcement in mm, A_v is area of all the bar legs in mm², and f_{yt} is the yield strength of the transverse punching shear reinforcement in MPa.

$$V_{EC} = 0.18\, K \sqrt[3]{100\, \rho_1\, f'_c}\; u_1\, d + 0.1\, f_{pc}\, u_1\, d + V_p + (1.5\, d\, A_{sw}\, f_{ywd,ef} \sin \alpha)/S_r \tag{2}$$

where V_{EC} is Ult. Punching shear capacity (N), k is $1 + \sqrt{200/d} \leq 2$, d is Effective depth of bonded tension reinforcement $= 0.5(d_x + d_y)$, where d_x and d_y are the effective depths of the bonded tension reinforcement in the *x* and *y* directions respectively, ρ_1 is the ratio of bonded tension reinforcement crossing the punching perimeter and can be taken as $(\rho_{lx} * \rho_{ly})^{0.5}$, where with the ratios ρ_{lx} and ρ_{ly} calculated for widths equal to those of the support plus three times the slab depth "3d" to each side, $\rho_1 \leq 0.02$, V_p is the sum of the vertical components of forces in tendons where they cross a perimeter of d/2 from the support face, $f_c`$ is the cylinder compressive strength of concrete ≤ 90 MPa, f_{pc} is Mean prestress compressive stresses along the critical perimeter after all losses ≤ 3.5 MPa, where s_r is the spacing of the shear reinforcement in mm, A_{sw} is the shear reinforcement area calculated in one perimeter around the column in mm², and $f_{ywd,ef}$ is the allowable design stress of the shear reinforcement in MPa given as: $f_{ywd,ef} = 250 + 0.25d \leq f_{ywd}$, and α is the angle formed by the shear reinforcement and the slab plane.

The theoretical punching capacities for the tested slabs were calculated according to ACI-318 and EC2 using Equations 1 and 2, and the values are summarized in Table 4 and graphically presented in Figure 10. These values indicated that the average deviations between test results and ACI provisions were about 1% and 6% for slabs without and with punching reinforcement, respectively. On the other hand, EC2 showed more conservative values, with average deviations of about 23% and 14% for slabs without and with punching reinforcement, respectively.

**Table 4. Experimental & theoretical punching capacities**

Slab	Pu Exp. kN	Pu ACI kN	$\dfrac{ACI}{Exp.}$%	Pu EC2 kN	$\dfrac{EC2}{Exp.}$%
S1	245.0	234.0	95.5%	200.0	81.6%
S2	274.7	270.5	98.5%	212.1	77.2%
S3	327.4	343.9	105.0%	235.8	72.0%
S4	271.4	268.6	98.9%	246.2	90.7%
S5	341.5	303.3	88.8%	292.3	86.6%
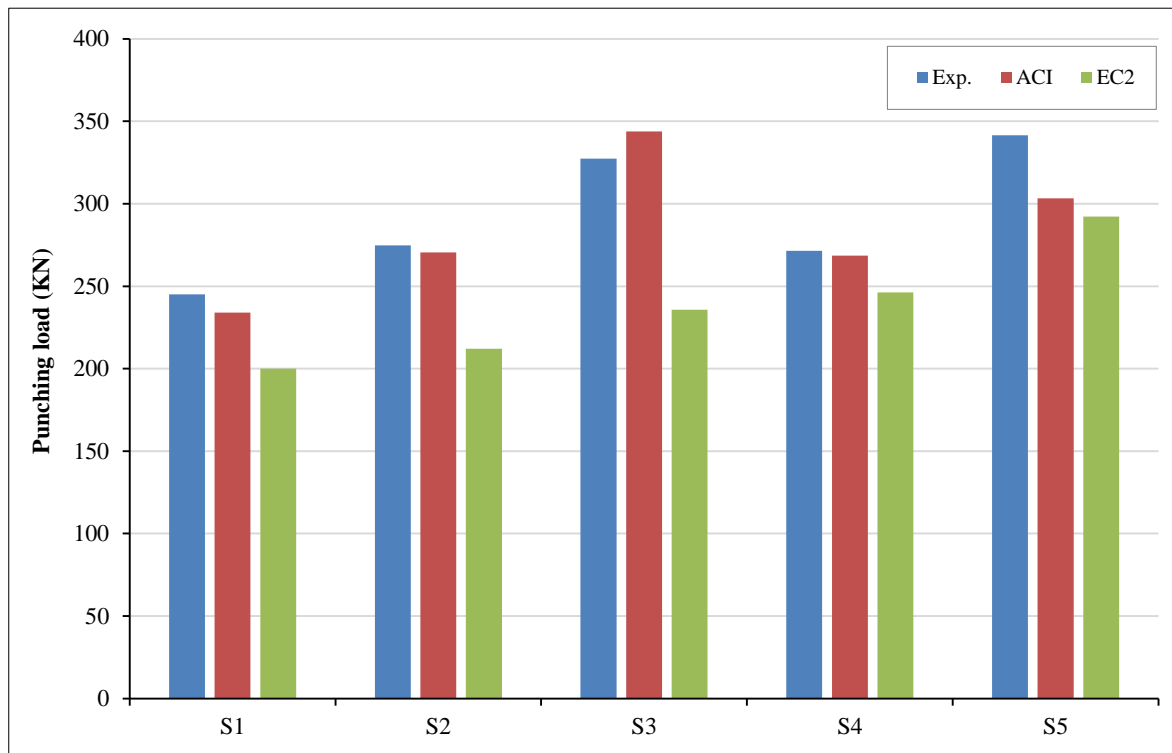
Figure 10. Punching capacities from tests' results, ACI-318 and EC2

The observed punching capacities shown in Table 3 present the following points:

- As expected, the punching capacity increased with the column dimension, as per the results of slabs S1, S2, and S3. However, the ultimate punching stress, considering the standard frustum angle in the ACI-318 (45°), decreases with increasing the aspect ratio of the column. This is a well-known phenomenon that is considered in the most design codes when using a reduction factor equals to (0.5+a/b) ≤1.0, where (a) is the column width and (b) is the column length. The calculated ultimate punching stress for S1, 2, and 3 based on the measured capacities are 4.08, 3.93, and 3.64 MPa, respectively, which correspond to reduction factors of 1.0, 0.96, and 0.89, respectively. Comparing these values with the codified ones (1.0, 1.0, and 0.75) indicates that the effect of column aspect ratio on the punching capacity of UHPC is less than its effect on normal strength concrete, as shown in Figure 11-a.

- The effect of the shear reinforcement ratio on the ultimate punching capacity is presented by slabs S1, S4, and S5. The presence of shear reinforcement in specimens S4 and S5 improved the punching capacity to about 111% and 140% of the unreinforced one (S1), respectively, as the shear reinforcement acts as dowels between the slab and the punching wedge. The measured results indicated that the punching capacity increased linearly with increasing the punching reinforcement area, as shown in Figure 11-b.

- The improved result of specimen S4 indicated that punching reinforcement is fully functional in UHPC even at spacing equal to 1.5 times the slab depth, compared with 1.0 times the depth for normal strength concrete in ACI-318.
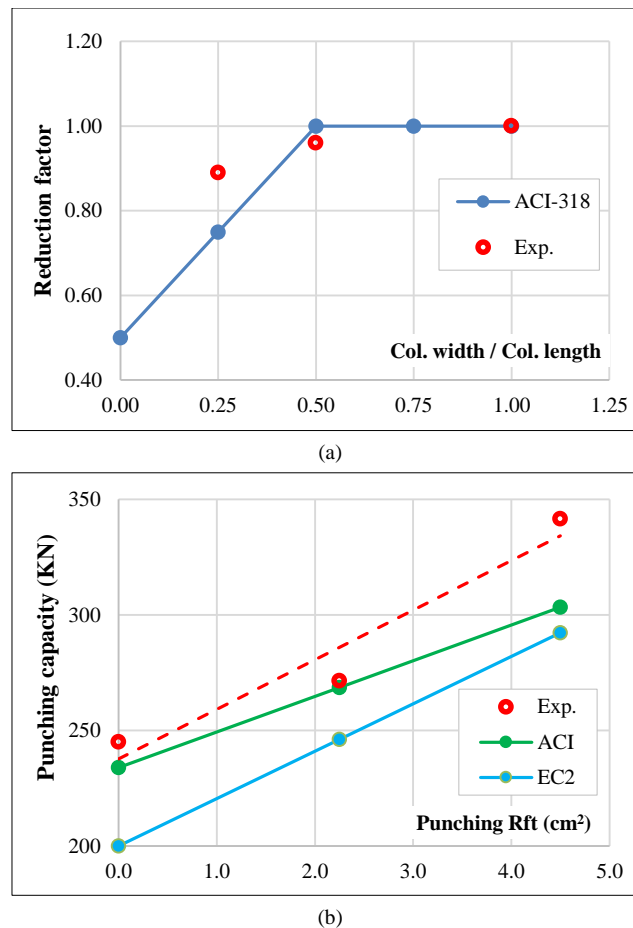
Figure 11. Analyzing the measured punching capacities, a) Comparing the experimental reduction factor due to column's aspect ratio with ACI-318 provisions b) Comparing the experimental impact of punching reinforcement on the capacity with ACI & EC2 provisions.

5.4. Load-Deflection

The presented load-deflection curves in Figure 12 summarize the behavior of each tested slab; analyzing these curves yields the following notes:

- Comparing the curves of S1, 4, and 5 indicated that both capacity and stiffness increased with increased punch reinforcement.

- Comparing the behavior of S1, S2, and S3 illustrates the effect of column dimensions. The curves showed that, as expected, the punching capacity increased with increasing the column dimensions; however, the large enhancement between S1 and S2 reflected that the reduction factor is almost the same (≈ 1.0). On the other hand, the slight difference between S2 and S3 capacities despite the large difference in column size indicates the low reduction factor of S3 (≈ 0.87).
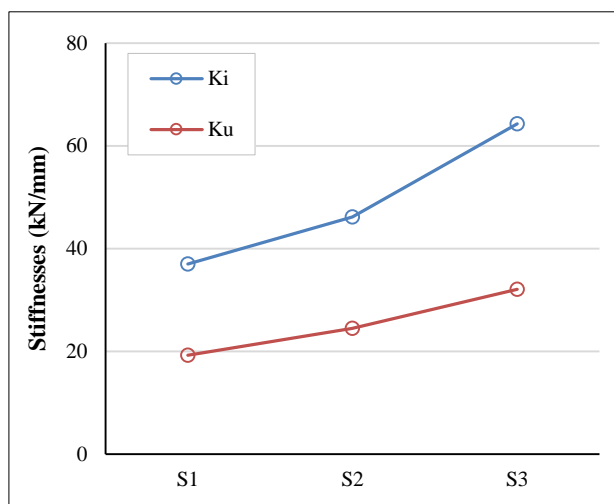
5.5. Stiffness

The initial stiffness of tested slabs before cracking (K_i) is calculated as the ratio between the maximum deflection at the cracking and ultimate stages. The initial stiffness (K_i) is highly affected by the column dimensions, as the slab S1 with column dimensions of 50×50 mm experienced the least initial stiffness of 37 kN/mm, while the same slabs with larger plate dimensions, as in slabs S2 and S3, experienced larger values of 46.20 kN/mm and 64.30 kN/mm, respectively. Also, the increase in the punching reinforcement ratio increased the initial stiffness, as slabs S4 and S5 achieved initial stiffnesses of 43.8 kN/mm and 45.2 kN/mm, respectively, which are 18.4% and 22.2% larger than the same slab without shear reinforcement (S1).

The stiffness of slabs decreases with loading due to crack propagation, reaching the ultimate stage in all tested specimens. Slabs with larger column dimensions showed higher ultimate stiffness, as slab S1 achieved an ultimate stiffness of 19.30 kN/mm, which is the least when compared with S2 and S3. Furthermore, slabs with shear reinforcement S4 and S5 experienced higher values of ultimate stiffness of 24.2 kN/mm and 28.7 kN/mm, respectively. The initial stiffness (K_i) and ultimate stiffness (K_u) are calculated for all tested flat slabs and summarized in Table 5.

Table 5. Stiffnesses and ductility of the tested slabs

Slab	Pcr kN	Pu kN	Δcr mm	Δu mm	Ki kN/mm	Ku kN/mm	μ
S1	100	245.0	2.7	12.7	37.0	19.3	4.7
S2	60	274.7	1.3	11.2	46.2	24.5	8.6
S3	90	327.4	1.4	10.2	64.3	32.1	7.3
S4	70	271.4	1.6	11.2	43.8	24.2	5.6
S5	95	341.5	2.1	11.9	59.4	28.7	7.4

(a)
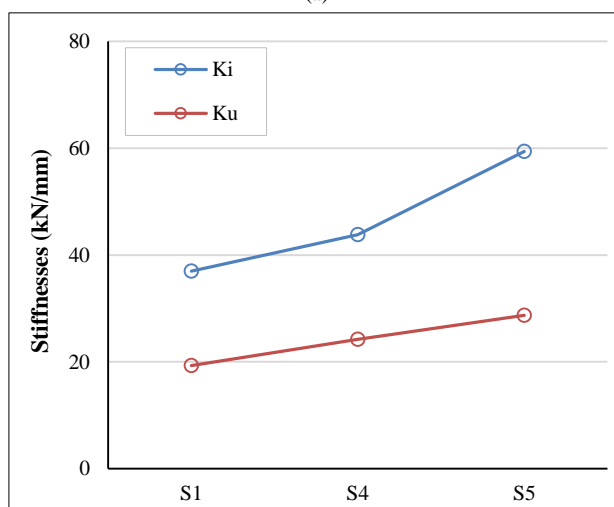
(b)

Figure 12. Analyzing the measured stiffnesses a) considering column size b) considering punching reinforcement

5.6. Ductility

The ductility of a slab is calculated as the ratio between the maximum deflections at the cracking and ultimate stages. As listed in Table 5, the ductility (μ) of all tested slabs exceeded 4. Moreover, the increase in column dimensions enhanced the ductility, as in S2 and S3, which achieved ductility of 8.6 and 7.3, respectively, compared with S1, which achieved 4.7. In addition, the punching reinforcement (S4 and S5) increased the slabs ductility by 48.9% and 21.3%, respectively, compared with S1.

5.7. Dissipated Energy

Dissipated energy is the area under the load-deflection curve. It represents the amount of damage exhibited by the slab until failure; hence, it is a good measurement for the seismic performance; the more dissipated energy, the more vibration damping, and accordingly, the better seismic performance. The measured dissipated energy values for the tested slabs are shown in Figure 13. All slabs showed almost the same amount of dissipated energy except S5, which showed an enhancement of about 20%.
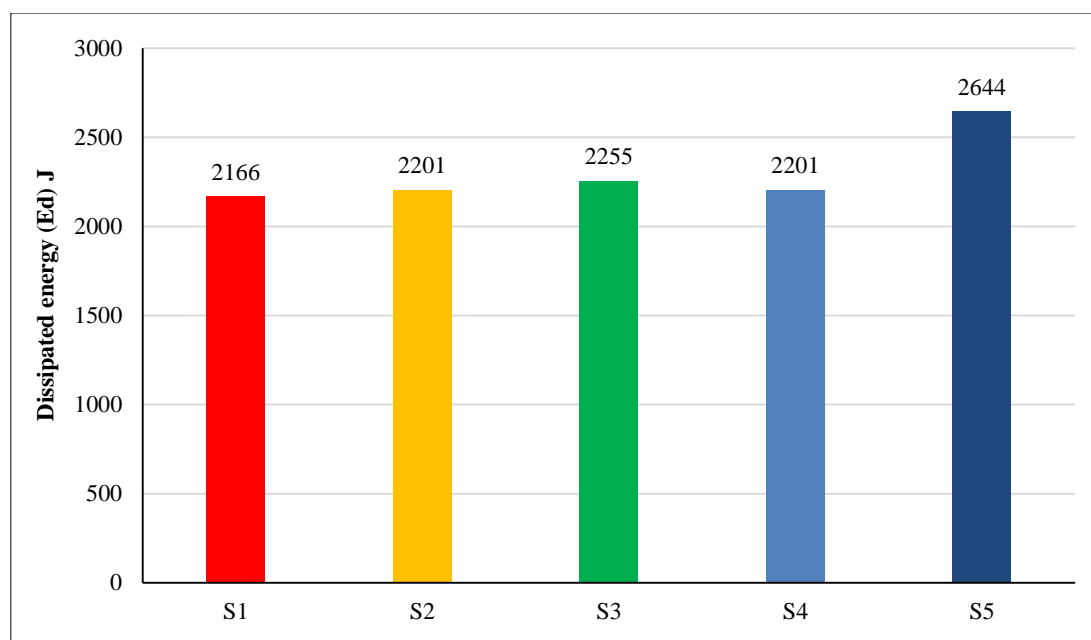
Figure 13. Dissipated energy values for the tested slabs

These results indicated that column dimension has a negligible effect on the dissipated energy. On the other hand, the enhanced dissipated energy of S5 due to the condiment of narrow pitched punching reinforcement (S = 0.75d) compared with the unenhanced dissipated energy of S4 with wide pitched punching reinforcement (S = 1.5d) illustrates the prime impact of punching reinforcement spacing on the seismic behavior of the slab.

6. Conclusions

This research aimed to investigate the effect of the column's aspect ratio and punching reinforcement ratio on the punching behavior of the UHPC posttensioned flat slab. An experimental program was conducted with five slabs (with a F_{cu} of 120 MPa). The experimental results were compared with the provisions of ACI-318 and EC2-2004. The outcomes of this research could be concluded in the following points:

- The failure pattern indicated that all slabs failed in punching. In addition, the use of punch reinforcement limited the crack propagation and increased the crack angle to 28° compared with 22° for the unreinforced slabs.

- The ultimate punching stress of UHPC post-tensioned slabs decreases with increasing the aspect ratio of the column, just like the normal strength concrete slabs but with smaller values, hence, it is recommended to replace the ACI reduction factor for normal strength concrete (0.5+a/b)≤1.0 with (0.6+a/b)≤ 1.0 for UHPC post-tensioned slabs.

- The contribution of punching reinforcement increased linearly with increasing the reinforcement ratio, which complies with the provisions of the design codes. In addition, the experimental results assured that the punching reinforcement is fully functioned even with spacing up to 1.5 times the slab depth due to the flat angle of pinching cracks of (28°).

- Both the ductility and stiffness of the UHPC flat slabs are enhanced with the increased column dimensions and punching reinforcement ratio.

- Comparing the experimental capacities with the calculated ones using ACI-318 and EC2 shows that ACI predictions are more accurate while EC2 predictions are more conservative. The average deviation percents were about 1% and 6% for ACI and 23% and 14% for EC2 for slabs without and with punching reinforcement, respectively.

- These conclusions are limited to slabs with F_{cu} up to 120 MPa subjected to concentrated static vertical loads only, without the effect of additional bending moments.

- Further study may be conducted to investigate the effect of other factors, such as the combined effect of vertical loads and bending moments, the behavior under cyclic loading, and the impact of using compressive strengths higher than 120 MPa.

7. Declarations

7.1. Author Contributions

Conceptualization, A.M.E.; methodology, D.M.O.; formal analysis, A.M.F.M.; investigation, M.R.; data curation, A.A.; supervision, A.H. All authors have read and agreed to the published version of the manuscript.

7.2. Data Availability Statement

The data presented in this study are available in the article.

7.3. Funding

The authors received no financial support for the research, authorship, and/or publication of this article.

7.4. Conflicts of Interest

The authors declare no conflict of interest.

8. References

[1] Al-Quraishi, H. A. A. (2014). Punching Shear Behavior of UHPC Flat Slabs. Ph.D. Thesis, The University of Kassel, Kassel, Germany.

[2] Ismail, M. (2015). Behavior of UHPC structural members subjected to pure torsion. Volume 24, Kassel University Press, Kassel, Germany.

[3] Abdujabborovich, M. R., & Ugli, N. N. R. (2016). Development and application of ultra-high performance concrete. Innovative Science, (5-2 (17)), 130-132. (In Russian).

[4] Elhegazy, H., Ebid, A., Mahdi, I., Haggag, S., & Abdul-Rashied, I. (2021). Implementing QFD in decision making for selecting the optimal structural system for buildings. Construction Innovation, 21(2), 345–360. doi:10.1108/CI-12-2019-0149.

[5] Elhegazy, H., Ebid, A. M., Mahdi, I. M., Aboul Haggag, S. Y., & Rashid, I. A. (2020). Selecting optimum structural system for R.C. multi-story buildings considering direct cost. Structures, 24, 296–303. doi:10.1016/j.istruc.2020.01.039.

[6] Einpaul, J., Bujnak, J., Ruiz, M. F., & Muttoni, A. (2016). Study on influence of column size and slab slenderness on punching strength. ACI Structural Journal, 113(1), 135–146. doi:10.14359/51687945.

[7] Sagaseta, J., Tassinari, L., Fernández Ruiz, M., & Muttoni, A. (2014). Punching of flat slabs supported on rectangular columns. Engineering Structures, 77, 17–33. doi:10.1016/j.engstruct.2014.07.007.

[8] Amin, M., Zeyad, A. M., Tayeh, B. A., & Agwa, I. S. (2022). Effect of ferrosilicon and silica fume on mechanical, durability, and microstructure characteristics of ultra-high-performance concrete. Construction and Building Materials, 320, 126233. doi:10.1016/j.conbuildmat.2021.126233.

[9] Azmee, N. M., & Shafiq, N. (2018). Ultra-high performance concrete: From fundamental to applications. In Case Studies in Construction Materials 9, 1–15. doi:10.1016/j.cscm.2018.e00197.

[10] Wu, X., Yu, S., Xue, S., Kang, T. H. K., & Hwang, H. J. (2019). Punching shear strength of UHPFRC-RC composite flat plates. Engineering Structures, 184, 278–286. doi:10.1016/j.engstruct.2019.01.099.

[11] Inácio, M. M. G., Lapi, M., & Pinho Ramos, A. (2020). Punching of reinforced concrete flat slabs – Rational use of high strength concrete. Engineering Structures, 206(110194), 1–13. doi:10.1016/j.engstruct.2020.110194.

[12] Menna, D. W., & Genikomsou, A. S. (2021). Punching Shear Response of Concrete Slabs Strengthened with Ultrahigh-Performance Fiber-Reinforced Concrete Using Finite-Element Methods. Practice Periodical on Structural Design and Construction, 26(1), 04020057–1 – 04020057–14. doi:10.1061/(asce)sc.1943-5576.0000546.

[13] Dogu, M., & Menkulasi, F. (2020). A flexural design methodology for UHPC beams posttensioned with unbonded tendons. Engineering Structures, 207(110193), 1–22. doi:10.1016/j.engstruct.2020.110193.

[14] Isufi, B., & Pinho Ramos, A. (2021). A review of tests on slab-column connections with advanced concrete materials. Structures, 32, 849–860. doi:10.1016/j.istruc.2021.03.036.

[15] Sharma, A., Thakur, P., Vashisht, R., & Shukla, A. (2022). Durability Evaluation of Normal and High Performance Concrete. Global Journal of Researches in Engineering, 22(1), 45–51. doi:10.34257/gjreevol22is1pg45.

[16] Muhammed, T. A., & Rahim Karim, F. (2022). The Influence of Drop Panel's Dimensions on the Punching Shear Resistance in Ultra-High-Performance Fiber-Reinforced Concrete Flat Slabs. Construction, 2(1), 55–65. doi:10.15282/construction.v2i1.7581.

[17] Elsayed, M., Abdel-Hady, I., Abdel-Hafez, L. M., & Tawfic, Y. R. (2022). Strengthening of slab-column connections using ultra high-performance fiber concrete. Case Studies in Construction Materials, 17(e01710), 1–12. doi:10.1016/j.cscm.2022.e01710.

[18] Gołdyn, M., & Urban, T. (2022). UHPFRC hidden capitals as an alternative method for increasing punching shear resistance of LWAC flat slabs. Engineering Structures, 271, 1–18. doi:10.1016/j.engstruct.2022.114906.

[19] Ebid, A., & Deifalla, A. (2022). Using Artificial Intelligence Techniques to Predict Punching Shear Capacity of Lightweight Concrete Slabs. Materials, 15(8), 2732. doi:10.3390/ma15082732.

[20] Elsheshtawy, S. S., Shoeib, A. K., Hassanin, A., & Ors, D. M. (2022). Influence of the Distribution and Level of Post-Tensioning Force on the Punching Shear of Flat Slabs. Designs, 7(1), 1. doi:10.3390/designs7010001.

[21] Ramadan, M., Ors, D. M., Farghal, A. M., Afifi, A., Zaher, A. H., & Ebid, A. M. (2023). Punching shear behavior of HSC & UHPC post tensioned flat slabs – An experimental study. Results in Engineering, 17, 100882. doi:10.1016/j.rineng.2023.100882.

[22] SIKA. (2019). SikaCem®-201 Intraplast: Additive for Cementitious Cable Grout. Product Data Sheet, SIKA, Nilai, Malaysia. Available online: https://mys.sika.com/dms/getdocument.get/07463d1b-e195-4a6f-b68d-d7f458a8f423/sikacem_-201_intraplast.pdf. (Accessed on January 2023).

[23] SIKA. (2014). Sika Fume®-HR Concrete Additive. Product Data Sheet, SIKA, Nilai, Malaysia. Available online: https://egy.sika.com/content/dam/dms/eg01/e/Sika%20Fume%20HR.pdf (Accessed on January 2023).

[24] SIKA. (2020). Sika® Quartz 02 IN: Quartz Based Broadcast Sand for Anti-Skid flooring Applications. Product Data Sheet, SIKA, Nilai, Malaysia. Available online: https://ind.sika.com/content/dam/dms/in01/h/sika_quartz_02_in.pdf (Accessed on January 2023).

[25] SIKA. (2015). Sika ViscoCrete®-3425: High Performance Superplasticiser Concrete Admixture. Product Data Sheet, SIKA, Nilai, Malaysia. Available online: https://egy.sika.com/content/dam/dms/eg01/e/Sika%20ViscoCrete%C2%AE%20-3425.pdf (Accessed on January 2023).

[26] BEKAERT. (2018). Bekinox® PES: Stainless steel fibers, blended with polyester fibers for anti-static and conductive textiles. BEKAERT, Zwevegem, Belgium. Available online: https://www.bekaert.com.cn/-/media/Brands2017/China/Files/CD022_Datasheet-PES.pdf?la=zh-CN (Accessed on January 2023).

[27] ASTM A416/A416M-06. (2010). Standard Specification for Steel Strand, Uncoated Seven-Wire for Prestressed Concrete. ASTM International, Pennsylvania, united States. doi:10.1520/A0416_A0416M-06.

[28] ACI 318M-14. (2014). Building Code Requirements for Structural Concrete and Commentary (ACI 318M-08). American Concrete Institute (ACI), Farmington Hills, United States.

[29] EN 1992-1-1. (2004). Eurocode2: Design of concrete structures. Part 1-1: General rules and rules for buildings. Brussels, Belgium.